J Appl Electrochem (2014) 44:353–360
DOI 10.1007/s10800-013-0648-9

RESEARCH ARTICLE

Improving the performance of silicon anode in lithium-ion batteries by Cu_2O coating layer

Si Hieu Nguyen · Jong-Choo Lim · Joong-Kee Lee

Received: 6 August 2013 / Accepted: 21 November 2013 / Published online: 1 December 2013

Abstract The influence of a 200 nm Cu_2O coating layer on the electrochemical performance of an 800 nm Si thin-film anode was investigated by cyclic voltammetry, electrochemical impedance spectroscopy, and galvanostatic charge/discharge measurements. The electrochemical performance of the Si thin-film anode was improved by the coating layer. The coated Si anode exhibited higher values of conductivity in comparison with the pristine Si anode. Scanning electron microscopy images of the anodes after cycling test showed that the coated Si anode after cycling test had less cracks than the pristine Si anode. The galvanostatic charge/discharge measurements reveal that the cyclability and rate capability of the coated Si thin-film anode were better than the pristine Si thin-film anode.

Keywords Lithium-ion batteries · Silicon anode · Cu_2O coating

1 Introduction

It is well known that the solid electrolyte interphase (SEI) plays an important role in the reversible cycling and long-term stability of graphite anodes in Li-ion batteries due to the surface passivation effect [1–4]. However, with silicon anodes—one of the best candidates for anode material in Li-ion batteries, the development of an SEI layer results in an opposite effect. During the intercalation process, the huge volume change (c.a. 300 %) of Li–Si alloy [5, 6] generates great mechanical stress and leads to the cracking of the Si anode material. Although the "self-welding" ability of Li–Si alloy has been confirmed [7], the formation of an SEI layer on the Si surface destroys this welding process. The SEI layer with the composition of oxides, organic–inorganic salt species [8, 9] will cover the surface of the cracks in alloy material, and hinders the patching process of the cracks in the Si anode. The formation of new cracks together with the development of old cracks results in the pulverization of the Si anode after a short period of time. To reduce the effect of the SEI layer on the performance of the Si anode, a protective layer on the surface of the Si anode is necessary. Several types of coating layers based on carbon [10, 11], conductive polymers [12], metallic oxides [13–17], and silicon alloy [18] have been shown to improve the performance of Si anodes. Generally, these coating layers not only protect the Si surface against the formation of SEI layer, but also increase the conductivity of Si anode.

Among metallic oxide semiconductors, cuprous oxide (Cu_2O) has been recognized as a candidate anode material in Li-ion batteries [19, 20]. Recently, many studies based on thin-film [21, 22], and nanostructures [23–27] of Cu_2O have shown the applicability of this material as a potential alternative anode material for Li-ion batteries. In another approach, Fu et al. [28] showed the protective effect of a Cu_2O layer, against the destruction of the propylene-carbonate-based electrolyte solution and the exfoliation of the graphite anode. In the case of Si anode material, a confirmation of the protective effect of the Cu_2O layers not only helps to improve the electrochemical performance of Si

S. H. Nguyen · J.-C. Lim
Department of Chemical and Biochemical Engineering, Dongguk University-Seoul, 3-26 Pil-Dong, Chung-Gu, Seoul 100-715, Korea

J.-K. Lee (✉)
Center for Energy Convergence, Korea Institute of Science and Technology, Hwarangno 14-gil 5, Seongbuk-gu, Seoul 136-791, Korea
e-mail: leejk@kist.re.kr

anode, but also gives a chance for the increase of specific capacity of Cu_2O anode material. In this paper, the contribution of the Cu_2O coating layer, on the electrochemical characteristics of amorphous Si thin-film anode, was investigated by cyclic voltammetry (CV) and electrochemical impedance spectroscopy (EIS). The composition of the coating layer, before and after lithiation, was studied by X-ray photoelectron spectroscopy (XPS) and Auger electron spectroscopy (AES). In addition, galvanostatic cycling tests and SEM observation were also performed to show the contribution of the Cu_2O layer to the stability of the Si anode structure.

2 Experimental

2.1 Preparation of materials

Amorphous Si thin films were first deposited on copper foil using an electron cyclotron resonance plasma-enhanced chemical vapor deposition (ECR-MOCVD) system. The plasma was generated by the electron cyclotron resonance of magnetic fields from two electromagnetic coils and a 2.45-GHz microwave source with a power of 700 W. For the preparation of the deposition process, the reaction chamber was pumped to a vacuum pressure of 10^{-5} torr by a turbo-molecular pump. During the deposition process, the working pressure was kept stable at 1.5×10^{-2} torr by a throttle valve. For the deposition of amorphous Si thin-film, the substrate temperature was kept at 200 °C, and a gas mixture of Ar and SiH_4 was used at flow rates of 30 and 5 sccm, respectively. After finishing the deposition of the Si thin-film, the sample was kept in the reaction chamber for the deposition of Cu_2O. The details of the deposition system can be found elsewhere [29]. The substrate temperature was kept at 250 °C. The flow rates of the (hfac) Cu (DMB), O_2, and Ar feeding gases were 5, 20, and 15 sccm, respectively. The deposition times of the amorphous Si and Cu_2O thin-films were 15 and 30 min, respectively. To protect the samples against oxidation, they were kept in an Ar environment, while the temperature was cooled down to room temperature by shutting off the heater.

2.2 Material characterization and electrochemical measurements

The morphology of the samples was observed using a Hitachi S-5500 scanning electron microscope (SEM). The crystal structure of the samples was investigated using a Bruker D8 X-ray diffractometer (XRD). The composition of the Cu_2O coating layer was analyzed by an Auger electron spectroscopy (AES) (ULVAC-PHI, AES-PHI 700) and an XPS-VG Scientific X-ray photoelectron spectroscope (XPS) with 27.9-W AlKα radiation at room temperature.

The half cells were fabricated in a dry room with humidity at a dew point less than −60 °C. An anode with an area of 2×2 cm^2 was separated from the Li electrode by a polyethylene separator. The liquid electrolyte was composed of 1 M $LiPF_6$ in ethylene carbonate, ethyl methyl carbonate, and dimethyl carbonate (1:1:1 volume ratio). Cyclic voltammetry (CV) and galvanostatic charge/discharge measurements were performed in the potential range of 0–2 V using a battery test system (Maccor Series 4000) at room temperature. The potential range CV analysis was carried out at a scan rate of 0.2 mV s^{-1}. The impedance measurements were carried out by an electrochemical impedance spectroscopy system (EIS-Zahner IM 6) at amplitude of 10 mV and frequency range of 10^{-2}–10^5 Hz. The "KK test for Windows" software was used to validate the quality of EIS data [30]. The deconvolution of impedance spectrum was performed by Tikhonov regularization method which implemented in the Ftikreg software [31, 32]. The fitting of EIS data was performed by Zview software.

3 Results and discussion

3.1 Structure and morphology

The cross section of the as-deposited Si thin films is shown in Fig. 1a. The Cu_2O crystals are pillar-shaped with diameters of about 20–50 nm. The thickness of the Si thin-film and Cu_2O layer were estimated at about 800 and 200 nm, respectively. XRD analysis was performed to determine the crystal structure of the deposited Si and Cu_2O thin-films. However, no diffraction peaks were observed in the XRD spectra. These results are similar with literatures [33, 34].

It is well known that XPS is a powerful technique for the study of transition metal compounds which have localized valence d orbitals. Figure 1b shows the XPS spectrum of Cu_2O coating layer. XPS peaks of Cu 2*p*1/2, Cu 2*p*3/2, and O 1*s* were detected at 952.4, 932.5, and 530.2 eV, respectively. Based on the disappearance of the satellite peak in the region of 946–938 eV [35] and the position of the O 1*s* peak [36], it can be concluded that the composition of the coating layer was Cu_2O.

3.2 Cyclic voltammograms

The effect of Cu_2O coating layer on the lithiation process of the Si thin-film anode was investigated by the cyclic voltammogram analysis. Figure 2a, b, respectively, present the cyclic voltammograms of the pristine Si thin-film and

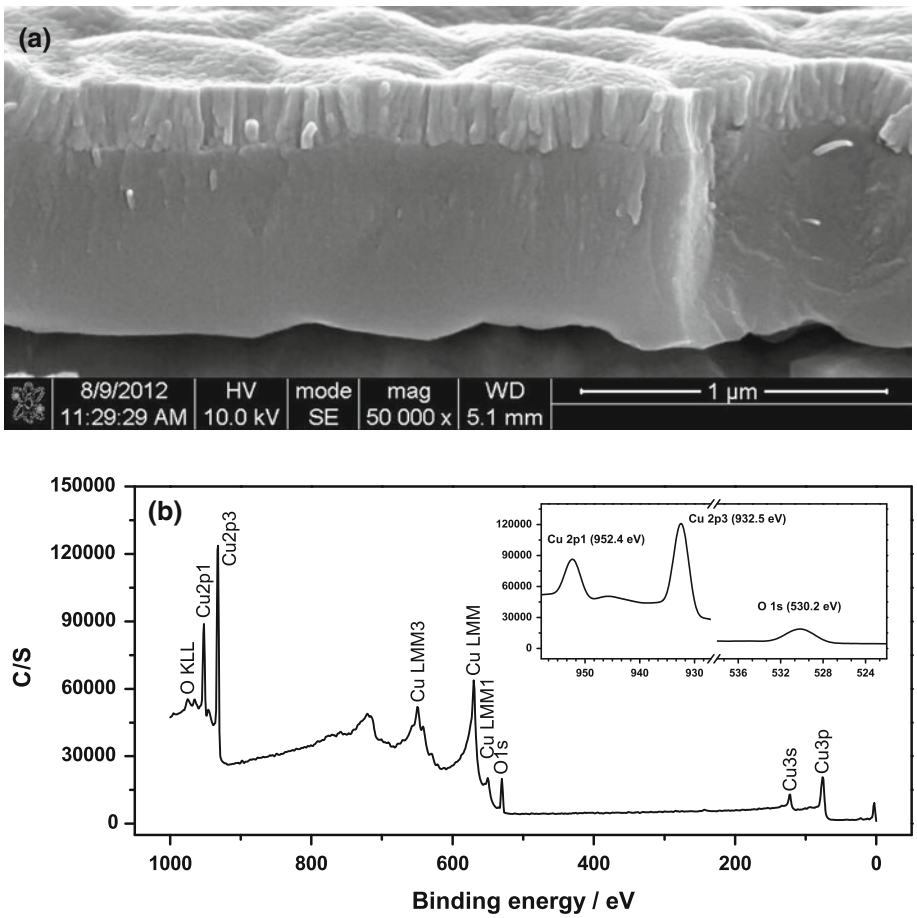

Fig. 1 **a** The cross section of copper-oxide-coated Si thin films. **b** The XPS spectrum of the copper oxide coating layer. The *inset* shows the detail of the Cu 2*p*1/2, Cu 2*p*3/2, and O 1*s* XPS peaks in the XPS spectrum of the Cu_2O coating layer

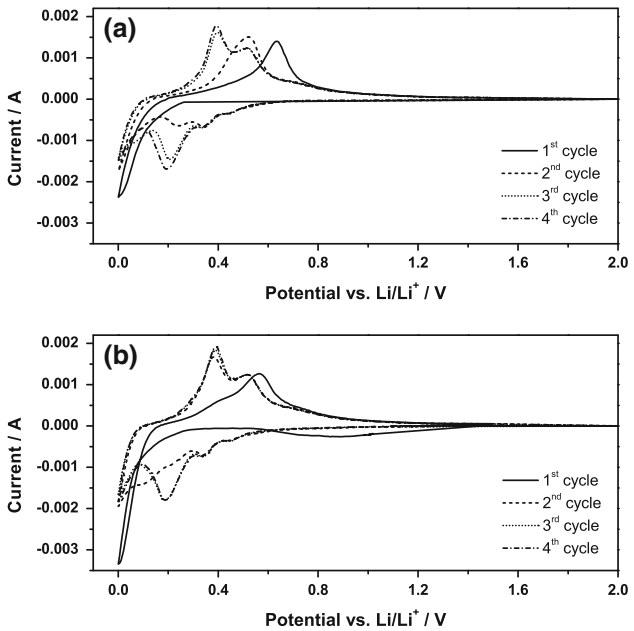

Fig. 2 The comparison of the cyclic voltammograms of the pristine Si thin-film (**a**) and the Cu_2O-coated Si thin-film (**b**) as electrodes at a scan rate of 0.2 mV s^{-1}

the Cu_2O-coated Si thin-film anodes obtained at a scan rate of 0.2 mV s^{-1}. Generally, the lithiation behavior of both samples was represented by four reduction peaks at around 0.42, 0.33, 0.19, and 0.02 V, and two broad oxidation peaks at around 0.52 and 0.39 V. However, the transformation of the cyclic voltammograms from the 1st cycle to the 4th was different between the two types of electrodes. In the case of the coated Si electrode, the cyclic voltammogram became stable after two cycles, while the pristine Si electrode needed three cycles to obtain the same result. This difference was even clearer in the oxidation behavior. Based on the Gibb's phase rule, the ambiguous present of lithiation peaks showed a behavior of nonuniform phase transformation in Si anode. At the same scan rate, the lower intensity of the oxidation peaks in the case of the pristine Si electrode revealed a lower intercalation level in comparison with the case of the pristine electrode.

A broad reduction peak at around 0.9 V, which showed at the first cycle, was assigned for the lithiation of the Cu_2O coating layer. The disappearance of this reduction peak at second cycle revealed that there was a change in the composition of the Cu_2O layer after the first cycle. This conclu-

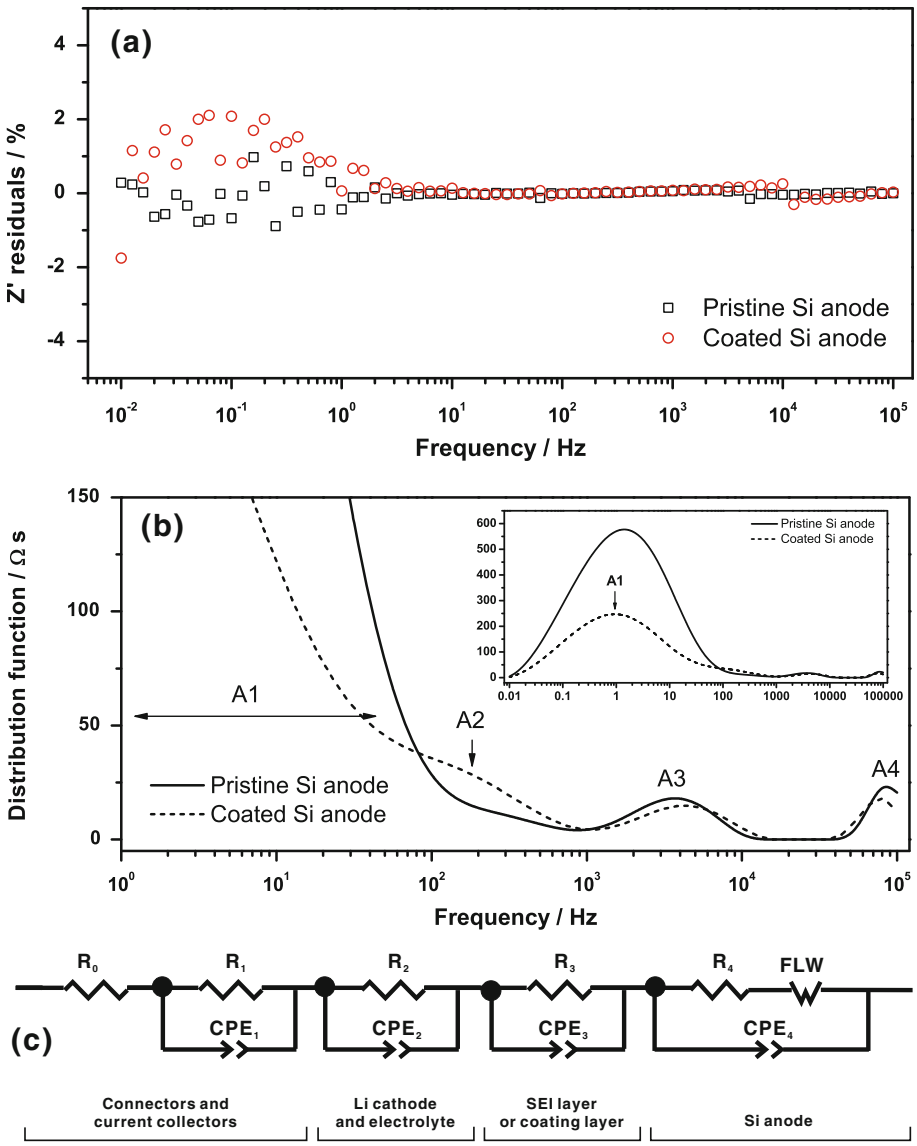

Fig. 3 **a** Kramers–Kronig residuals of real impedance of the pristine and the Cu_2O-coated Si cells. **b** DRT spectra of the pristine and the Cu_2O-coated Si cells after 20 cycles of charge/discharge. The *inset* shows the spectra at full scale of frequency. **c** The equivalent circuit used to fit impedance data

sion was supported by the observation of George and co-authors [37] recently. In that work, the authors pointed out that the lithiation process of Cu_2O was quite complex, and there were tiny Cu particles which existed after cycling test. Herein, AES analysis was performed to look for the existence of Cu metal in the coating layer after first cycle of charge/discharge. However, the AES spectra of the coating layer did not show any change in the Cu LMM Auger peak [38]. There was evidence for the extension of the Auger spectra of Cu clusters by size effect [39]. This size effect may results in an overlap of the Cu LMM peaks in the Auger spectra.

3.3 Electrochemical impedance spectroscopy

The effect of the Cu_2O coating layer on the electrical conductivity and surface properties of the Si thin-film anodes was examined by electrochemical impedance spectroscopy. Figure 3a shows results of the Kramers–Kronig (K–K) transform tests of the pristine and coated Si thin-film anode. With residuals are mainly below 1 %, the quality of EIS data is acceptable [40]. In this work, the calculation of the distribution of relaxation times (DRT) of electrochemical impedance spectra was performed to analyze EIS data [31, 32]. The DRT spectra of the pristine and coated Si anodes after 20 cycles of charge/discharge are presented in Fig. 3b. Generally, there are four impedance arcs which can be identified by the DRT technique. At low frequency, the diffusion of Li^+ ion into Si anode was attributed to A1 peak. By comparison of two spectra, A2 peak was assigned for the coating layer to the impedance spectrum. In the range of very high frequency, the existence of A4 peak might come from the contribution of connectors and current collectors. The last contribution from electrolyte and Li cathode was assigned to A3 peak.

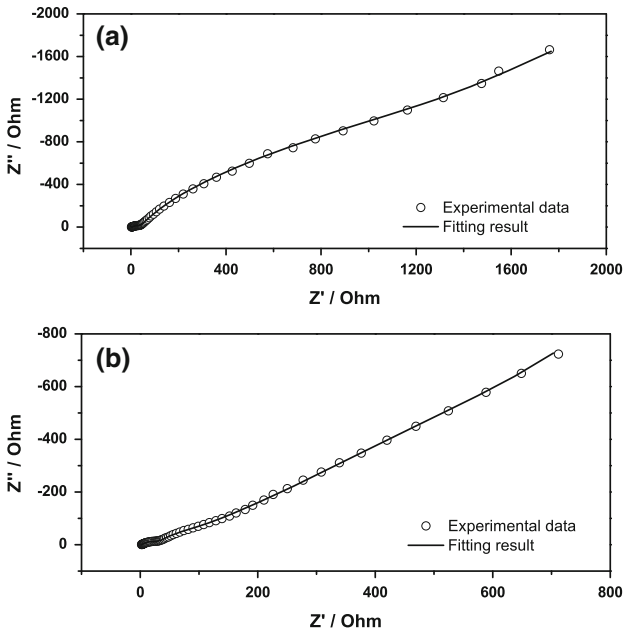

Fig. 4 The Nyquist plot and the fitting result of the pristine Si thin-film cell (**a**) and the Cu_2O-coated Si thin-film cell (**b**)

For further investigation, the DRT analyses of the half cells were performed at different sizes of Si anodes. However, the DRT spectra showed the changes in intensity of all DRT peaks at the different sizes of Si anode.

The equivalent circuit for EIS fitting was showed in Fig. 3c, the diffusion of Li^+ ion into Si anode was modeled by a Finite Length Warburg (FLW) element which can be presented as follow:

$$Z_{\mathrm{FLW}} = R_{\mathrm{W}}(j\omega\tau)^{-\alpha}\tan h(j\omega\tau)^{\alpha} \quad (1)$$

The value of α in Eq. (1) is in the range of 0–1. R_{W} is constant, and τ is the time constant of the diffusion process (proportional to l^2/D, where l and D are the thickness of the inserted thin-film and the diffusion coefficient of Li^+ ions, respectively).

The Nyquist plots of the pristine and coated Si thin-film anodes were presented in Fig. 4a, b, respectively. The equivalent circuit showed good fitting results. The fitting results for resistance (R4) and diffusion coefficient of the pristine anode are 1,999 Ω and 1.4×10^{-10} cm^2 s^{-1}, respectively. In the case of the coated Si anode, these values, respectively, are 74 Ω and 1.42×10^{-10} cm^2 s^{-1}. Although there was no improvement in the diffusivity of the coating anode, it is clear that the conductivity of the pristine Si anode were improved by Cu_2O coating layer.

The DRT analysis also used to investigate the variation of electrical properties of the Si anodes during cycling test. Figure 5a showed the DRT spectra of the pristine Si anodes after 20, 30, and 60 cycles of charge/discharge at 0.5 C rate. During cycling test, the A2 peak increased and moved to the low frequency region. The increase in intensity of this peak showed the development of the SEI layer during cycling test. This behavior was different with the case of the coated electrode. In Fig. 5b, the intensity of A2 peak decreased with the increase of cycle number. After 60 cycles of charge/discharge, the shape of A2 peak becomes clearer. This fact may results from the formation of an SEI layer on the surface of the coating layer. The increase in the total impedance of the coated anode after 60 cycles of charge/discharge in Fig. 5d may caused by the contributions of SEI layer and the poor contact of active material. In Fig. 5c, the decrease in the total impedance of the pristine anode together with the decrease of the specific capacity after 60 cycles of charge/discharge may results from the loss of active material due to cracking after cycling test.

3.4 Cycling performances

The cycling performance of the Cu_2O-coated Si thin-film anode in comparison with the pristine Si thin-film anode is presented in Fig. 6. Galvanostatic cycling tests were performed between 0 and 2 V (vs. Li/Li^+) at 0.5 C rate. For the calculation of the specific capacity of the thin-film anodes, the weight of the active material was estimated by the densities of Cu_2O (6 g cm^{-3}) [41] and amorphous silicon (2.2 g cm^{-3}) [42]. The voltage profiles of the pristine and the coated anodes at first three cycles are presented in Fig. 6a, b, respectively. At the first cycle, the specific charge and discharge capacities of the pristine Si anodes, respectively, were 2,673 and 2,380 mAh g^{-1}. In the case of the coated Si anode, the specific charge and discharge capacities at the first cycle were 1,994 and 1,610 mAh g^{-1}, respectively. As can be seen from figure, the lithiation behavior of the Cu_2O coating layer (at around 1.5 V) almost disappeared after first cycle of charge/discharge. The low value of coulombic efficiency at the first cycle and the disappearance of the lithiation behavior of the Cu_2O coating layer at the second cycle may be caused by the irreversible lithiation reaction in the Cu_2O coating layer.

Figure 6c showed the cyclability of the pristine and the coated Si anodes. The fading process of the pristine Si anode after more than 20 cycles of charge/discharge was presented by the decrease of the charging capacity and the coulombic efficiency. It is clear that the cyclability of Si thin-film anode was improved by the coating layer. After 100 cycles of charge/discharge, the charging capacities of the coated and the pristine Si anode, respectively, were 509 and 342 mAh g^{-1}. The rate capability of the Si anodes was presented in Fig. 6d. The C-rate values were calculated based on the current which applied on the cells at 1 C. The coated Si anode exhibited a better rate performance in comparison with the pristine Si anode.

The structural stability of the pristine and coated Si thin-film anodes was observed by the SEM observations.

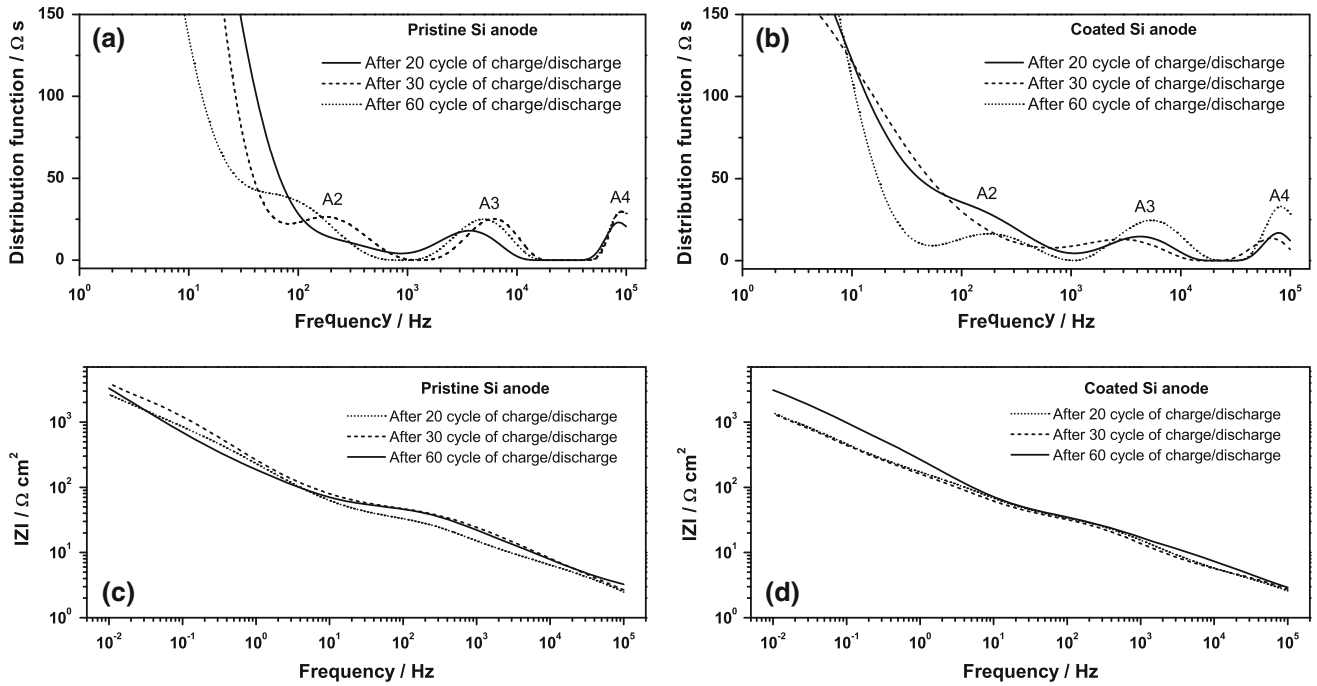

Fig. 5 DRT spectra of the pristine and the Cu_2O-coated Si cells (**a**) and the Cu_2O-coated Si thin-film cell (**b**) after 20, 30, and 60 cycles of charge/discharge. Magnitude of impedance of the pristine and the Cu_2O-coated Si cells (**c**) and the Cu_2O-coated Si thin-film cell (**d**) after 20, 30, and 60 cycles of charge/discharge

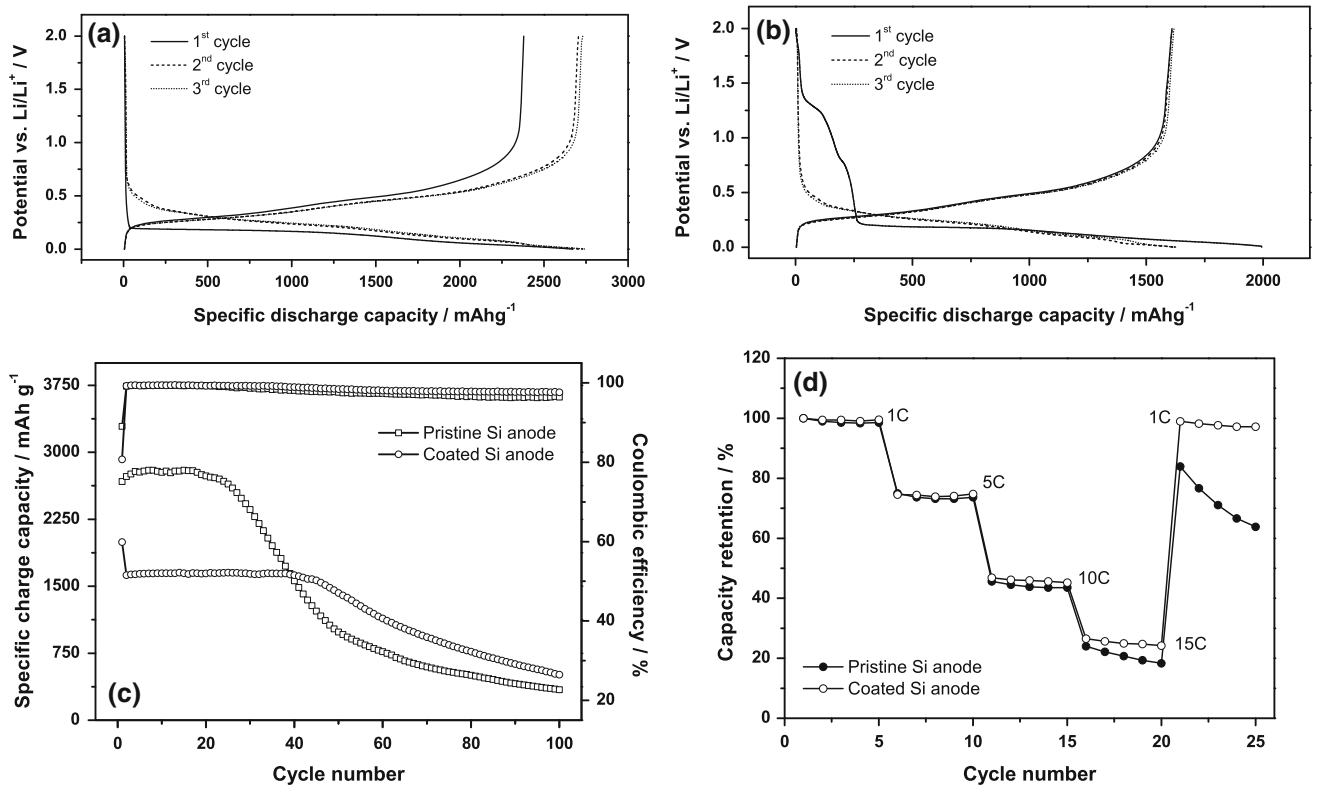

Fig. 6 Profiles of voltage versus capacity for the pristine Si thin-film anode **a** the Cu_2O-coated Si thin-film anode **b** during first 3 cycles. **c** Comparison of cycling behavior and coulombic efficiency of the pristine Si thin-film and the Cu_2O-coated Si thin-film anodes. **d** Comparison of rate capability of the pristine Si thin-film and the Cu_2O-coated Si thin-film anodes

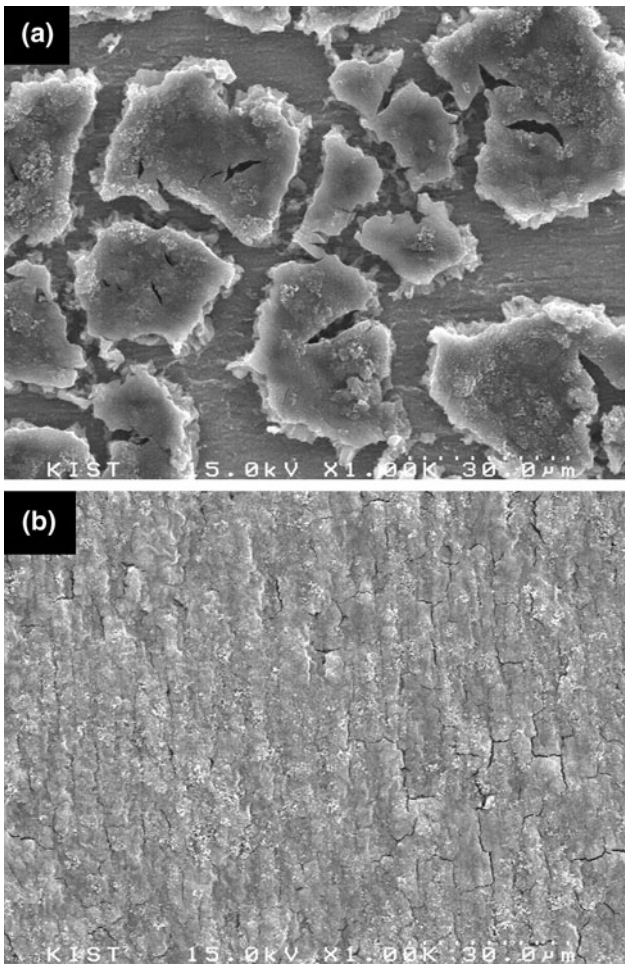

Fig. 7 SEM morphology of **a** the pristine Si thin-film and **b** the Cu_2O-coated Si thin-film anodes after 30 cycles of charge/discharge

Figure 7a, b, respectively, showed SEM images of the pristine and Cu_2O-coated Si thin-film anodes after 30 cycles of charge/discharge. In contradiction with the case of pristine Si thin-film anode, where the anode was cracked and separated into many islands about 10–40 μm in size, the structure of Cu_2O-coated Si thin-film anode was quite stable after cycling test. As can be seen in Fig. 7b, only small cracks can be observed on the surface of coated Si thin-film anode even after 30 cycles of charge/discharge. The stable in the structure resulted in the better electrochemical performance of the coated Si thin-film anode in comparison with the pristine Si thin-film anode. As can be concluded from CV and EIS analysis, the Cu_2O coating layer helped to improve the uniformity of the phase transformation processes. This uniform phase transformation might result in the decrease of the stress in the coated Si thin-film anode. In addition, the coating layer also protected Si surface against the formation and the development of the SEI layer on the surface of the Si thin-film anode and finally resulted in the longer lifetime and the improvement of the stability of structure of the Cu_2O-coated Si thin-film anode during cycling test.

4 Conclusion

The coating of Cu_2O layer on the amorphous Si thin-film anode resulted in the improvement in the electrochemical performance of Si thin-film anodes. This benefit caused by the effects of coating layer on the increase of surface conductivity and the restriction of the SEI layer formation. Although there was no evidence for the change in the composition of the Cu_2O coating layer after cycling test, we believe that the existence of the Cu tiny particles which was confirmed in the literature resulted in the improvement of surface conductivity of the coated Si thin-film anodes. As a result, the improvement of surface conductivity helped to improve the lithiation behavior of the coated Si thin-films. Moreover, the coating layer also helped to increase the uniformity of the phase transformation process, and finally resulted in the decrease of stress inside the Si thin-film anodes. Overall, the results in this paper have shown the applicability of the Cu_2O coating layer for the improvement of the electrochemical performance of Si anodes in Li-ion batteries.

Acknowledgments This work was supported by KIST institutional program and research grants (NRF-2012MIA2A2761792) funded by the National Research Foundation under the Ministry of Science, ICT & Future, Korea.

References

1. Peled E (1979) The electrochemical behavior of alkali and alkaline earth metals in nonaqueous battery systems—the solid electrolyte interphase model. J Electrochem Soc 126:2047–2051. doi:10.1149/1.2128859
2. Aurbach D, Markovsky B, Weissman I, Levi E, Ein-Eli Y (1999) On the correlation between surface chemistry and performance of graphite negative electrodes for Li ion batteries. Electrochim Acta 45:67–86. doi:10.1016/S0013-4686(99)00194-2
3. Zheng T, Gozdz AS, Amatucci GG (1999) Reactivity of the solid electrolyte interface on carbon electrodes at elevated temperatures. J Electrochem Soc 146:4014–4018. doi:10.1149/1.1392585
4. Herstedt M, Abraham DP, Kerr JB, Edström K (2004) X-ray photoelectron spectroscopy of negative electrodes from high-power lithium-ion cells showing various levels of power fade. Electrochim Acta 49:5097–5110. doi:10.1016/j.electacta.2004.06.021
5. Huggins RA (1988) Lithium alloy negative electrodes formed from convertible oxides. Solid State Ion 113–115:57–67. doi:10.1016/S0167-2738(98)00275-6
6. Obrovac MN, Christensen L, Le DB, Dahn JR (2007) Alloy design for lithium-ion battery anodes. J Electrochem Soc 154:A849–A855. doi:10.1149/1.2752985
7. Karki K, Epstein E, Cho JH, Jia Z, Li T, Picraux ST, Wang C, Cumings J (2012) Lithium-assisted electrochemical welding in silicon nanowire battery electrodes. Nano Lett 12:1392–1397. doi:10.1021/nl204063u

8. Chan CK, Ruffo R, Hong SS, Cui Y (2009) Surface chemistry and morphology of the solid electrolyte interphase on silicon nanowire lithium-ion battery anodes. J Power Sources 189:1132–1140. doi:10.1016/j.jpowsour.2009.01.007
9. Catarina PN, Światowska J, Chagnes A, Ozanam F, Gohier A, Pierre TV, Cojocaru CS, Cassir M, Marcus P (2013) Interphase chemistry of Si electrodes used as anodes in Li-ion batteries. Appl Surf Sci 266:5–16. doi:10.1016/j.apsusc.2012.10.165
10. Cui LF, Yang Y, Hsu CM, Cui Y (2009) Carbon–silicon core–shell nanowires as high capacity electrode for lithium ion batteries. Nano Lett 9:3370–3374. doi:10.1021/nl901670t
11. Arie AA, Vovk OM, Lee JK (2010) Surface-coated silicon anodes with amorphous carbon film prepared by fullerene C60 sputtering. J Electrochem Soc 157:A660–A665. doi:10.1149/1.3363531
12. Yao Y, Liu N, McDowell MT, Pasta M, Cui Y (2012) Improving the cycling stability of silicon nanowire anodes with conducting polymer coatings. Energy Environ Sci 5:7927–7930. doi:10.1039/C2EE21437G
13. He Y, Yu X, Wang Y, Li H, Huang X (2011) Alumina-coated patterned amorphous silicon as the anode for a lithium-ion battery with high coulombic efficiency. Adv Mater 23:4938–4941. doi:10.1002/adma.201102568
14. Yoo H, Lee JI, Kim H, Lee JP, Cho J, Park S (2011) Helical silicon/silicon oxide core–shell anodes grown onto the surface of bulk silicon. Nano Lett 11:4324–4328. doi:10.1021/nl202417c
15. Wu H, Chan G, Choi JW, Ryu I, Yao Y, McDowell MT, Lee SW, Jackson A, Yang Y, Hu L, Cui Y (2012) Stable cycling of double-walled silicon nanotube battery anodes through solid-electrolyte interphase control. Nat Nanotechnol 7:310–315. doi:10.1038/nnano.2012.35
16. Nguyen HT, Zamfir MR, Duong LD, Lee YH, Bondavalli P, Pribat D (2012) Alumina-coated silicon-based nanowire arrays for high quality Li-ion battery anodes. J Mater Chem 22:24618–24626. doi:10.1039/C2JM35125K
17. Jeon BJ, Lee JK (2011) Electrochemical characteristics of porous TiO_2 encapsulated silicon anode. Electrochim Acta 56:6261–6265. doi:10.1016/j.electacta.2011.05.056
18. Park O, Lee JI, Chun MJ, Yeon JT, Yoo SM, Choi SH, Choi NS, Park SJ (2013) High-performance Si anodes with a highly conductive and thermally stable titanium silicide coating layer. RSC Adv 3:2538–2542. doi:10.1039/C2RA23365G
19. Poizot P, Laruelle S, Grugeon S, Dupont L, Tarascon JM (2000) Nano-sized transition-metal oxides as negative-electrode materials for lithium-ion batteries. Nature 407:496–499. doi:10.1038/35035045
20. Grugeon S, Laruelle S, Urbina RH, Dupont L, Poizot P, Tarascona JM (2001) Particle size effects on the electrochemical performance of copper oxides toward lithium. J Electrochem Soc 148:A285–A292. doi:10.1149/1.1353566
21. Xiang JY, Tu JP, Huang XH, Yang YZ (2008) A comparison of anodically grown CuO nanotube film and Cu_2O film as anodes for lithium ion batteries. J Solid State Electrochem 12:94–945. doi:10.1007/s10008-007-0422-1
22. Xiang JY, Wang XL, Xia XH, Zhang L, Zhou Y, Shi SJ, Tu JP (2010) Enhanced high rate properties of ordered porous Cu_2O film as anode for lithium ion batteries. Electrochim Acta 55:492–4925. doi:10.1016/j.electacta.2010.03.091
23. Lee YH, Leu IC, Liao CL, Chang ST, Wu MT, Yen JH, Fung KZ (2006) Fabrication and characterization of Cu_2O nanorod arrays and their electrochemical performance in Li-ion batteries. Electrochem Solid State Lett 9:A207–A210. doi:10.1149/1.2171815
24. Fu LJ, Gao J, Zhang T, Cao Q, Yang LC, Wua YP, Holze R, Wu HQ (2007) Preparation of Cu_2O particles with different morphologies and their application in lithium ion batteries. J Power Sources 174:1197–1200. doi:10.1016/j.jpowsour.2007.06.030
25. Xiang JY, Tu JP, Yuan YF, Huang XH, Zhou Y, Zhang L (2009) Improved electrochemical performances of core–shell Cu_2O/Cu composite prepared by a simple one-step method. Electrochem Commun 11:262–265. doi:10.1016/j.elecom.2008.11.029
26. Kang W, Liu F, Su Y, Wang D, Shen Q (2011) The catanionic surfactant-assisted syntheses of 26-faceted and hexapod-shaped Cu_2O and their electrochemical performances. CrystEngComm 13:4174–4280. doi:10.1039/C1CE05319A
27. Zhang Z, Chen H, She X, Sun J, Teo J, Su F (2012) Synthesis of mesoporous copper oxide microspheres with different surface areas and their lithium storage properties. J Power Sources 217:336–344. doi:10.1016/j.jpowsour.2012.05.088
28. Fu LJ, Gao J, Zhang T, Cao Q, Yang LC, Wu YP (2007) Effect of Cu_2O coating on graphite as anode material of lithium ion battery in PC-based electrolyte. J Power Sources 171:904–907. doi:10.1016/j.jpowsour.2007.05.099
29. Chang WY, Choi JW, Lim JC, Lee JK (2010) Effects of ZnO coating on electrochemical performance and thermal stability of $LiCoO_2$ as cathode material for lithium-ion batteries. J Power Sources 195:320–326. doi:10.1016/j.jpowsour.2009.06.104
30. Boukamp BA (1995) A linear Kronig–Kramers transform test for immittance data validation. J Electrochem Soc 142:1885–1894. doi:10.1149/1.2044210
31. Weese J (1992) A reliable and fast method for the solution of Fredhol integral equations of the first kind based on Tikhonov regularization. Comput Phys Commun 69:99–111. doi:10.1016/0010-4655(92)90132-I
32. Sonn V, Leonide A, Ivers-Tiffée E (2008) Combined deconvolution and CNLS fitting approach applied on the impedance response of technical Ni/8YSZ cermet electrodes. J Electrochem Soc 155:B675–B679. doi:10.1149/1.2908860
33. Bruno G, Capezzuto P, Madan A (1995) Plasma deposition of amorphous silicon-based materials. Academic Press, San Diego
34. Holzschuh H, Suhr H (1990) Deposition of copper oxide (Cu_2O, CuO) thin-films at high temperatures by plasma-enhanced CVD. Appl Phys A Mater Sci Process 51:486–490. doi:10.1007/BF00324731
35. Panzner G, Egert B, Schmidt HP (1985) The stability of CuO and Cu_2O surfaces during argon sputtering studied by XPS and AES. Surf Sci 151:400–408. doi:10.1016/0039-6028(85)90383-8
36. Ghijsen J, Tjeng LH, van Elp J, Eskes H, Westerink J, Sawatzky GA, Czyzyk MT (1988) Electronic structure of Cu_2O and CuO. Phys Rev B 38:11322–11330. doi:10.1103/PhysRevB.38.11322
37. Paolella A, Brescia R, Prato M, Povia M, Marras S, Trizio LD, Falqui A, Manna L, George C (2013) Colloidal synthesis of cuprite (Cu_2O) octahedral nanocrystals and their electrochemical lithiation. ACS Appl Mater Interfaces 5:2745–2751. doi:10.1021/am4004073
38. Larson PE (1974) X-ray induced photoelectron and auger spectra of Cu, CuO, Cu_2O, and Cu_2S thin-films. J Electron Spectrosc Relat Phenom 4:213–218. doi:10.1016/0368-2048(74)80052-6
39. de Crescenzi M, Diociaiuti M, Lozzi L et al (1986) Size effects on the linewidths of the Auger spectra of Cu clusters. Surf Sci 178:282–289. doi:10.1016/0039-6028(86)90304-3
40. Scully JR, Silverman DC, Kendig MW (1993) Electrochemical impedance: analysis and interpretation. American Society for Testing and Materials, Philadelphia, p 154
41. Hodgman CD (1962) Handbook of chemistry and physics. Cleveland, Chemical Rubber Co., p 572
42. Tan SI, Berry BS, Crowder BL (1972) Elastic and anelastic behavior of ion-implanted silicon. Appl Phys Lett 20:88–90. doi:10.1063/1.1654060